Structure and Bonding of Solvated Mercury(II) and Thallium(III) Dihalide and Dicyanide Complexes by XAFS Spectroscopic Measurements and Theoretical Calculations

Ralf Åkesson,[†] Ingmar Persson,[‡] Magnus Sandström,*[,†] and Ulf Wahlgren[§]

Department of Chemistry, The Royal Institute of Technology, S-100 44 Stockholm, Sweden, Department of Chemistry, Swedish University of Agricultural Sciences, P.O. Box 7015, S-750 07 Uppsala, Sweden, and Department of Physics, Stockholm University, P.O. Box 6730, S-113 85 Stockholm, Sweden

Received January 28, 1994[⊗]

The solvation of mercury(II) complexes and ions has been studied by XAFS methods and compared to the corresponding thallium(III) species. Analyses of Hg L_{III} edge extended X-ray absorption fine structure (EXAFS) spectra gave the distances 2.29(2) and 2.31(2) Å for $HgCl_2$ in aqueous and dimethyl sulfoxide solutions, respectively, 2.46(2) Å for solid $HgBr_2$ and 2.42(2) Å for $HgBr_2$ in aqueous solution; for $Hg(CN)_2$ in aqueous solution Hg–C = 2.04(2) Å and Hg–N = 3.18(3) Å. The weakness of the EXAFS signals observed of the solvated Hg^{2+} ion in e.g. pyridine, acetonitrile, and aqueous solutions are interpreted as being due to dynamic distortions of the first solvation shell by second-order Jahn–Teller effects. The pre-edge transitions in the X-ray absorption near-edge structure (XANES) region for mercury(II) and thallium(III) complexes have been used to distinguish between different coordination geometries of the solvated species. Theoretical *ab initio* calculations have been performed on the structures of the mercury(II) and thallium(III) dihalide and dicyanide complexes, in order to compare the effects of differences in bonding and hydration, and also on the valence shell energy levels, to assist assignments of pre-edge features in the XANES spectra. Relativistic effective core potentials (ECP) were constructed, both for the ground-state mercury and thallium atoms and for the 2p ionized state, and used in calculations at the MCPF level of bond lengths and relative energy differences. The first pre-edge peak found for all complexes in their XANES spectra was assigned to a (2p) → Σ_g^+ (~Hg 6s) excitation, with the splitting of the pre-peak for $Hg(CN)_2$ possibly due to (2p) → Π^*(C–N) at ca. 3.4 eV higher energy. Multiple scattering resonances have been discussed for the CN ligands. Comparisons of calculated and experimental bond lengths of the mercury(II) and thallium(III) dichloride and dicyanide complexes revealed unexpectedly short bond lengths for the mercury(II) complexes, which have been discussed in terms of weaker solvation and stronger bonding. The bonding in the $Hg(CN)_2$ and $Tl(CN)_2^+$ complexes were analyzed by theoretical calculations using a constrained space orbital variation (CSOV) technique, showing significant contributions of back-donation particularly in the Hg–CN bonds. The trends of the force constants from vibrational spectra are consistent with this picture and show stronger and shorter M–C bonds but also stronger C–N bonds in the $Hg(CN)_2$ complex than in the $Tl(CN)_2^+$ complex.

Introduction

The purpose of this study was to obtain additional structural information on the solvation and bonding of the mercury(II) ion and some neutral mercury(II) complexes in solvents with different coordinating ability:[1] water, acetonitrile, dimethyl sulfoxide (Me_2SO), and pyridine (py). EXAFS (Hg L_{III} edge) spectra have been measured in order to obtain distances between mercury and the atoms in its first coordination sphere. The pre-edge transitions of the XANES region have been analyzed with assignments partly based on theoretical *ab initio* calculations, designed to predict the energies of the electronic transitions from the Hg 2p level (*i.e.* the Hg L_{III} edge) in $HgCl_2$ and $Hg(CN)_2$. For comparisons, theoretical calculations have also been made on the corresponding isoelectronic thallium(III) complexes, which, together with previously obtained structural results, have been used to achieve a better understanding of some unique features in the coordination chemistry of mercury(II).

Previously, the solvation of the mercury(II) ion in Me_2SO and aqueous solutions has been studied by large-angle X-ray scattering (LAXS).[2] In both solvents the radial distribution function (RDF) showed a broad peak corresponding to six Hg–O bonds, although with an unexpectedly large variation in the distance. The hexasolvation was further corroborated by the Hg–S peak in the RDF for the Me_2SO solution and by crystal structure determinations of $[Hg(H_2O)_6](ClO_4)_2$, $[Hg(Me_2SO)_6](ClO_4)_2$, and $[Hg(py)_6](CF_3SO_3)_2$, crystallized from saturated solutions.[3-5]

Thermodynamic data indicate an extensive desolvation at the formation of the first and second complexes between the hexasolvated mercury(II) ion and halide or cyanide ligands,[6] with an unusually large range of stability of the second complexes.[7] LAXS and EXAFS techniques have previously been used to study the structures of HgX_2 complexes in solution.[8,9] Hg–Cl distances of 2.35 Å (LAXS)[8] and 2.32 Å (EXAFS)[9] and Hg–Br = 2.45 Å (LAXS)[8] were obtained for the solvated HgX_2 complexes in Me_2SO. A large amount of experimental results (Raman, IR, EXAFS, LAXS)[8-10] confirm that the Me_2SO molecules coordinate *via* the oxygen atom to mercury. However, the solvent molecules are loosely coordinated and the Hg–O distances,

[†] The Royal Institute of Technology.
[‡] Swedish University of Agricultural Sciences.
[§] Stockholm University.
[⊗] Abstract published in *Advance ACS Abstracts,* July 15, 1994.
(1) Sandström, M.; Persson, I.; Persson, P. *Acta Chem. Scand.* **1990,** *44,* 653 and references therein.
(2) Sandström, M.; Persson, I.; Ahrland, S. *Acta Chem. Scand. Ser. A* **1978,** *32,* 607.
(3) Johansson, G.; Sandström, M. *Acta Chem. Scand. Ser. A* **1978,** *32,* 109; **1987,** *41,* 113.
(4) Sandström, M.; Persson, I. *Acta Chem. Scand. Ser. A* **1978,** *32,* 95.
(5) Akesson, R.; Sandström, M.; Stålhandske, C.; Persson, I. *Acta Chem. Scand. Ser. A* **1991,** *45,* 165.
(6) Dash, K. C.; Kinjo, Y.; Persson, I. *Acta Chem. Scand.* **1990,** *44,* 433.
(7) Ahrland, S.; Ishiguro, S.-I.; Marton, A.; Persson, I. *Acta Chem. Scand. Ser. A* **1985,** *39,* 227.
(8) Sandström, M. *Acta Chem. Scand. Ser. A* **1978,** *32,* 627 and references therein.
(9) Persson, I.; Penner-Hahn, J. E.; Hodgson, K. O. *Inorg. Chem.*, submitted for publication.
(10) Persson, I.; Sandström, M.; Goggin, P. L. *Inorg. Chim. Acta* **1987,** *129,* 183 and references therein.

0020-1669/94/1333-3715$04.50/0

Table 1. EXAFS Results: Interatomic Distances, d, Mean Square Deviations, σ^2, and Number of Distances, n, from the Metal Atom in a Complex[a]

sample	complex	distance	d/Å[b]	$10^{-3}\sigma^2$/Å^2	n[d]
$HgCl_2$(s)[e]	$HgCl_2$	Hg–Cl	2.29	3.4	2
0.23 M $HgCl_2$(aq)[e]	$HgCl_2$(aq)	Hg–Cl	2.296[g]	3.3	2
0.24 M $HgCl_2$(aq)[e,h]	$HgCl_2$(aq)	Hg–Cl	2.292[g]	1.8	2
1.0 M $HgCl_2(Me_2SO)$[e]	$HgCl_2(Me_2SO)$	Hg–Cl	2.314[g]	4.4	2
		Hg–O	2.65(5)	25	4
$HgBr_2$(s)[e]	$HgBr_2$	Hg–Br	2.46	3.7	2
0.016 M $HgBr_2$(aq)[e]	$HgBr_2$(aq)	Hg–Br	2.417	2.4	2
0.016 M $HgBr_2$(aq)[f]	$HgBr_2$(aq)	Hg–Br	2.420	3.2	2
0.25 M $Hg(CN)_2$(aq)[f]	$Hg(CN)_2$(aq)	Hg–C	2.02[i]	–0.2[j]	2
		Hg–N	3.16(3)[i]	0.2[j]	2
0.5 M $TlCl_2(ClO_4)$(aq)[e,h]	$TlCl_2(aq)^+$	Tl–Cl	2.37	4.0	2
		Tl–O	2.32	16	4
0.5 M $TlBr_2(ClO)_4$(aq)[e,h]	$TlBr_2(aq)^+$	Tl–Br	2.46	3.3	2
		Tl–O	2.38	12	4
1.4 M $Tl(CN)_2(ClO_4)$(aq)[f,h]	$Tl(CN)_2(aq)^+$	Tl–C	2.11[k]	–1.6[j]	2
		Tl–O	2.42	8[j]	4
		Tl–N	3.25[k]	–0.7[j]	2

[a] Thallium data from ref 14. [b] Estimated error ±0.02 Å (±0.04 Å for Tl–O) if not otherwise indicated. [c] Estimated error ±1 × 10^3 Å^2 (±3 × 10^3 for M–O) in σ^2. [d] n is kept constant. [e] Theoretical EXAFS parameters by FEFF. [f] Model-based EXAFS parameters. [g] Based on Hg–Cl = 2.282 Å.[22] [h] SSRL data. [i] Based on Hg–C = 2.019 Å and Hg–N = 3.18 Å [26] from $Hg(CN)_2$(s). [j] Relative to the (unknown) σ^2 value of the model compound: $\sigma^2_{sample} - \sigma^2_{model}$. [k] Fixed from LAXS results.[14]

estimated to ca. 2.5 Å (LAXS)[8] and 2.6 Å (EXAFS)[9] for $HgCl_2$ and ca. 2.65 Å for $HgBr_2$ (LAXS),[8] are difficult to determine precisely. Also for other solvents, e.g. methanol (Hg–Cl = 2.31, Hg–O ~ 2.66 Å)[8] and pyridine (Hg–Cl = 2.375, Hg–N = 2.47 Å),[11] bond distances have been obtained by the LAXS method, but for most solvents only indirect information from Raman spectroscopy and comparisons with crystal structure data of solid solvates are available.[10]

The Hg–X bond distances of the solvated HgX_2 molecules generally increase with increasing coordinating ability of the solvent with a corresponding shift of the Hg–X symmetric stretching vibrational frequency (ν_s) toward lower wavenumbers.[1,10] Raman spectroscopic measurements of the wavenumber difference, $\tilde{\nu}_s[HgBr_2(g)] - \tilde{\nu}_s[HgBr_2(solvent)]$, have been used to construct the donor strength (D_s) scale, giving a measure of the electron-pair donating ability (Lewis basicity) of the solvents.[1,10] A corresponding gradual decrease is also found in the X–Hg–X angle, which is close to 180° in the gas phase and in noncoordinating solvents, whereas for solvent molecules with extreme coordinating ability (e.g. phosphines) X–Hg–X angles below tetrahedral (<109.5°) are reached.[10]

It has been proposed that the pronounced preference in mercury(II) coordination chemistry to form two opposite strong and short *trans* bonds is a result of the rather small energy separation between the valence shell 6s and the occupied $5d_{z^2}$ atomic Hg orbitals, giving some d-character to the binding molecular orbitals because of configurational mixing.[12] For the hexasolvates a vibronic coupling of the corresponding electronic states occurs, which can be described as a second-order (or pseudo) Jahn–Teller (SOJT) effect.[13] This reduces the stability of the octahedral coordination and causes an increase in the amplitude of the stretching vibration of E_g symmetry. In structural studies of the solvated ion in solution this effect appears as an anomalously large Debye–Waller factor.[13]

An EXAFS study of the isoelectronic thallium(III) ion was performed on the same occasion as the present SSRL study, and some close similarities, particularly concerning the features of the XANES regions, but also deviating behavior can be found between the systems.[14] The higher charge of thallium markedly increases the solvation, and the hydrated Tl^{3+} ion is octahedrally coordinated in a $[Tl(H_2O)_6]^{3+}$ complex with a mean Tl–O distance of 2.23 Å,[15] whereas the linear TlX_2^+ species were found to be hydrated by four water molecules with Tl–O distances increasing from ca. 2.3 to 2.4 Å for X = Cl, Br, and CN, respectively.[14] The M–O bond of the $[Hg(H_2O)_6]^{2+}$ ion in aqueous solution is much longer, 2.41 Å,[2] than that of $[Tl(H_2O)_6]^{3+}$, 2.23 Å.[15] For the weakly hydrated HgX_2 complexes neither Hg–O distances nor hydration numbers have been possible to obtain by structure studies. The gradual transition toward pseudotetrahedral HgX_2L_2 complexes with more strongly coordinating solvents L [10] is probably a unique feature for mercury(II) (cf. CuX_2^- complexes which do not show the same behavior).[16] Although no structural studies of TlX_2^+ complexes so far have been made in nonaqueous solvents, a similar tendency is not expected.

Methods

Sample Preparation. The solutions were prepared by dissolving weighed amounts of mercuric chloride, bromide, and cyanide (Merck, analytical grade) in the dried solvents. It is well-known that the neutral HgX_2 complex will strongly dominate under these conditions.[6] High solubility and a low degree of ion-pair formation are required for structure studies of the solvation of Hg^{2+} in nonaqueous solvents, and for this purpose the $CF_3SO_3^-$ and CF_3COO^- anions were used. The solutions studied by EXAFS are given in Table 1. The mercury concentration was in the range 0.25–1.0 M for all solutions except for the aqueous solution of $HgBr_2$, for which only 0.016 M could be attained. Some pyridine and acetonitrile solutions were also investigated, although only the XANES region was found to be informative. The concentrations of the saturated solutions of $Hg(CF_3SO_3)_2$ and $Hg(CF_3COO)_2$ in pyridine were 0.016 and 0.2 M, respectively. The solid disolvate $[Hg(py)_2](ClO_4)_2$ was prepared by gentle heating of the hexasolvate $[Hg(py)_6](ClO_4)_2$ as described before.[5,17]

EXAFS Measurements. Hg L_{III}-edge X-ray absorption data were collected in transmission mode at ambient temperature at the Synchrotron Radiation Source, SRS, Daresbury Laboratory, Warrington, U.K., under dedicated conditions (2.0 GeV, 100–200 mA) using the wiggler station 9.2, and at the SSRL synchrotron radiation source at Stanford, CA (3.0 GeV, 40–100 mA). Si(220) and Si(111) double monochromators were used at the SRS and SSRL experiments, respectively, detuned to 50% of maximum intensity in order to suppress higher order harmonics. The

(11) Persson, I.; Sandström, M.; Goggin, P. L.; Mosset, A. *J. Chem. Soc., Dalton Trans.* **1985**, 1597.
(12) (a) Orgel, L. E. *J. Chem. Soc.* **1958**, 4186. (b) Nyholm, R. S. *J. Chem. Soc., Proc.* **1961**, 273.
(13) Strömberg, D.; Sandström, M.; Wahlgren, U. *Chem. Phys. Lett.* **1990**, *172*, 49.
(14) Blixt, J.; Glaser, J.; Mink, J.; Persson, I.; Persson, P.; Sandström, M. Unpublished results.
(15) Glaser, J.; Johansson, G. *Acta Chem. Scand.* **1981**, *35*, 639; **1982**, *36*, 125.
(16) Persson, I.; Sandström, M.; Steel, A. T.; Zapatero, M. J.; Akesson, R. *Inorg. Chem.* **1991**, *30*, 4075.
(17) Chudinova, L. I. *J. Appl. Chem. USSR* **1969**, *42*, 161; *Russ. J. Inorg. Chem.* **1969**, *14*, 1568.

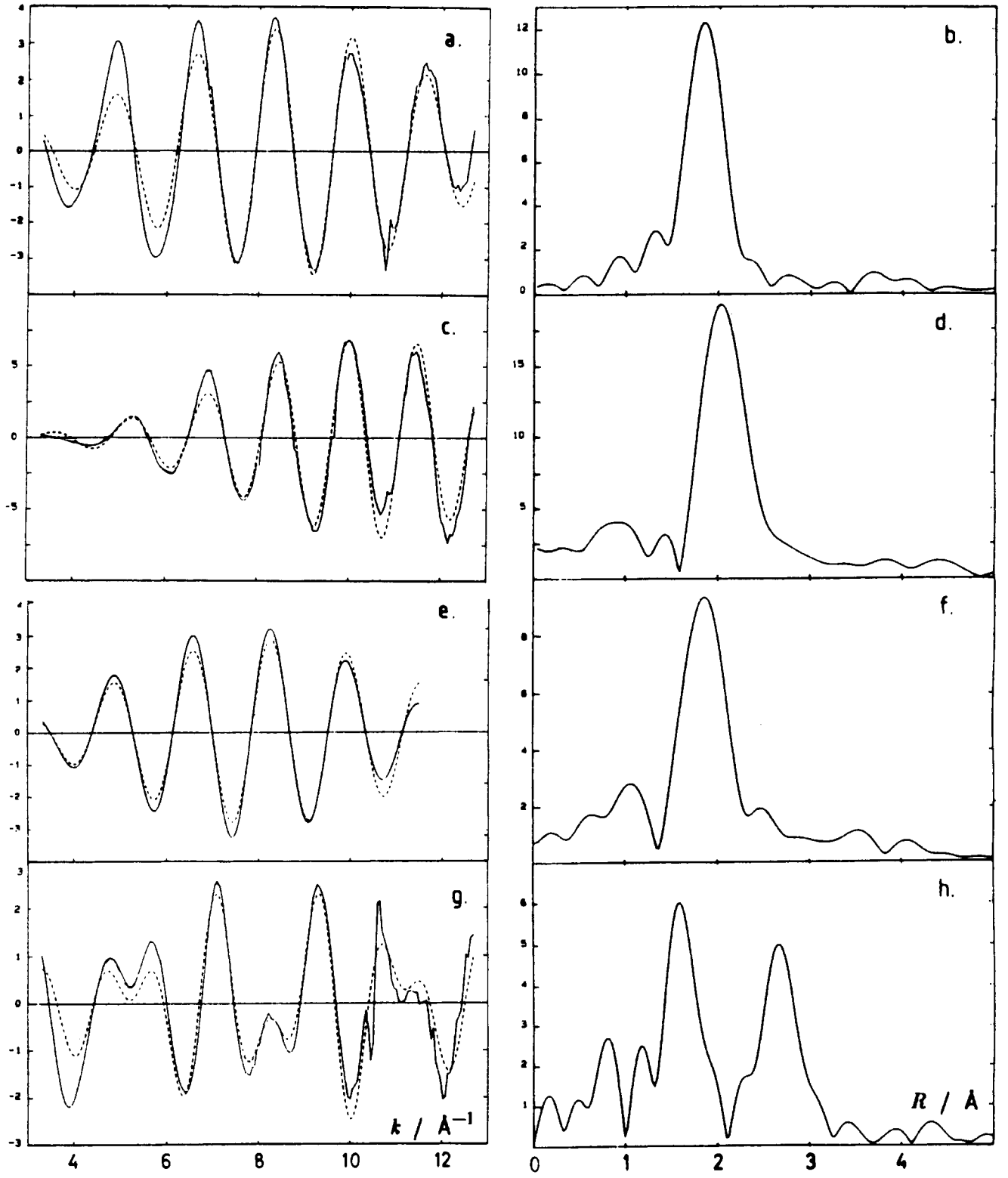

Figure 1. EXAFS: Curve-fitting (dashed curves, parameters from Table 1) of unfiltered k^3-weighted EXAFS data (solid line) and corresponding Fourier transforms of (a, b) $HgCl_2(aq)$, (c, d) $HgBr_2(aq)$, (e, f) $HgCl_2(Me_2SO)$, and (g, h) $Hg(CN)_2(aq)$.

energy scale of all spectra was calibrated by simultaneously recording the L_{III} edge of $HgCl_2$ assigned to 12 282 eV.[9] Solution cells with Mylar or thin (~50 μm) glass windows and Vitone or Teflon spacers (0.5–2 mm, 0.1 mm for Me_2SO) were used.

EXAFS data were extracted usually on 3–4 averaged scan files, using standard procedures of pre-edge subtraction,[18] spline removal,[19] and Fourier filtering,[18] by means of the computer program packages XFPAKG[19] or EXAFSPAK.[20a] In the range 3 to ~14 Å^{-1} of the scattering variable k, EXAFS data weighted by k^3 were used for the Fourier-transform and curve-fitting procedures (Figure 1). In the EXAFSPAK program system theoretical back-scattering parameters were generated by the FEFF program,[20b] while for the XFPAKG program package transferability of the phase shift and amplitude parameters of a specific element from model compounds of similar chemical structure was assumed.[21] In order to extract EXAFS interaction parameters from

(18) (a) Sayers, D. E.; Bunker, B. A. In *X-Ray Absorption: Principles, Applications, Techniques of EXAFS, SEXAFS and XANES*; Koningsberger, D. C., Prins, R., Eds.; Wiley-Interscience: New York, 1988; Chapter 6. (b) Durham, P. J. *Ibid.*, Chapter 2.5. (c) Bianconi, A. *Ibid.*, Chapter 11. (d) Bianconi, A.; Dell'Ariccia, M.; Durham, P. J.; Pendry, J. B. *Phys. Rev.* **1982**, *26*, 6502.
(19) Scott, R. A. *Meth. Enzymol.* **1985**, *117*, 414.

the model compounds for the Hg–Cl, Hg–Br, Hg–N(or O), and Hg–C and Hg–N(2nd shell) distances in linear (Hg–C–N) configuration, EXAFS spectra were recorded for the solids $HgCl_2$, $HgBr_2$, $[Hg(py)_2](ClO_4)_2$, and $Hg(CN)_2$, diluted with boron nitride to obtain a suitable (about one logarithmic unit) absorption change over the edge. The reported bond distances in the model compounds are the following: Hg–Cl = 2.282 Å,[22] Hg–Br = 2.49 Å,[23,24] and Hg–N = 2.12 Å from the $Hg(py)_2(CF_3COO)_2$ structure.[25] Solid $Hg(CN)_2$ has an Hg–C bond length of 2.019 Å (corrected for thermal motion) and a nearly linear (177°) Hg–C–N geometry, corresponding to an Hg–N distance of 3.18 Å.[26] By using the experimental second shell Hg···N interaction to extract back-scattering parameters for the nitrogen atom the increased back-scattering capacity of the N-atom in a linearly coordinated CN ligand due to multiple scattering[18d] is approximately accounted for.

The fit of the models to some of the unfiltered EXAFS spectra is shown in Figure 1. In all cases the final curve fitting was performed with the coordination numbers fixed at the expected values.

Theoretical Calculations. Quantum chemical *ab initio* calculations have been performed with the SCF and the size-consistent MCPF[27] (modified coupled pair functional) methods. All excitations out of the metal d shell and the valence shell of the ligand orbitals (including 2s on C and N and 3s on Cl) using a single-configuration reference state were included in the expansion of the wave function.

The Hg and Tl atoms were described using an effective core potential (ECP) basis set, with the 1s–4s, 2p–4p, 3d, 4d, and 4f orbitals included in the core.[28] Relativistic effects were accounted for by parametrizing the ECP to an atomic relativistic all-electron wave function, (^{3}P; $d^{10}sp$) for mercury and (^{2}P; $d^{10}s^2p$) for thallium. The all-electron basis sets were slightly extended versions of the atomic basis set of Faegri.[29] The relativistic method used in the atomic calculations was the spin-free no-pair external field method proposed by Douglas and Kroll[30] and implemented by Hess.[31] At the ECP level a (9s8p7d3f) primitive basis set was used for the mercury and thallium atoms. This basis set was obtained by a least-squares fitting procedure to the all-electron atomic valence orbitals. In most of the applications the primitive ECP basis set was contracted by means of the ANO procedure[32] to ⟨4s3p3d2f⟩, using the natural orbital coefficients obtained from an MCPF calculation on the ions Hg^+ (^{2}S; $d^{10}s^1$) and Tl^+ (^{1}S; $d^{10}s^2$) in the uncontracted basis.

Oxygen and nitrogen were described using Dunning's (9s5p) basis set,[33] augmented by one p and one d function, and contracted to ⟨3s4p1d⟩. For chlorine an (12s9p) atomic basis set was used,[34] augmented with one diffuse p function ($e^{0.044}$) and five primitive d functions.[35] The sp part of this basis was Raffenetti contracted[36] to ⟨4s4p⟩, while the five d-functions were contracted to one, using the ANO procedure.[32]

Two different ECP's and ANO basis sets were constructed for mercury. The first one described a neutral Hg atom, and the second, a mercury ion with a hole in the 2p shell. The 2p orbital in Hg has a very small spatial extent, with an $\langle r^2 \rangle$ value of $0.005a_0$,[37] and the ionized atom can thus to a good approximation be mimicked simply by increasing the nuclear charge of Hg by one unit.

The bond distances in the HgX_2 and TlX_2^+ systems were optimized by assuming a linear geometry ($D_{\infty h}$). The energies of the allowed (2p) → Σ_g^+ and (2p) → Π_g transitions relative to the 2p ionization potential were calculated using the ECP describing an ionized Hg atom and compared with the XANES pre-edge transitions. Calculations were also carried out on the reference compounds HCN and HCl.

Results and Discussion

I. EXAFS. The EXAFS results, *i.e.* bond distances and their mean-square deviations (σ^2) with estimated errors and coordination numbers (n, kept constant in the refinements), including results for some corresponding thallium(III) solutions for comparisons,[14] are summarized in Table 1. The fit of the calculated curves to the unfiltered data and the Fourier transforms are given in Figure 1.

Solvated Hg^{2+}. The hexaaquamercury(II) ion, for which the mean Hg–O distances in solution previously have been determined to 2.41(1) Å by the LAXS method,[2] has also been studied in the solid state. A crystal structure determination of $[Hg(H_2O)_6](ClO_4)_2$ gave six equivalent bonds with Hg–O distances of 2.341(6) Å (2.35 Å after correction for thermal "riding" motion).[3] The longer bond distance in solution is probably related to the larger anharmonicity caused by the second-order Jahn–Teller (SOJT) effect.[13] This is consistent with the rapidly decreasing amplitude of the EXAFS signals for aqueous mercury(II) perchlorate solutions. The isoelectronic hexahydrated Tl^{3+} ion does not show similar effects, and virtually the same Tl–O distance, 2.23 Å, was found in solution and in the solid state,[15] corresponding to well-defined EXAFS spectra.[14]

A similar Hg–O distance (2.40 Å), as in the X-ray solution study, was also obtained in a theoretical SCF calculation using effective core potentials (ECP) for the inner orbitals of the mercury atom,[13] although the omission of correlation effects should have caused a slight elongation of the calculated distance. The SOJT effect causes a flattening of the ground-state potential surface, corresponding to an enlarged amplitude of the E_g stretching vibration.[13] The difference between the experimental Hg–O and Tl–O bond distances for the hexahydrated isoelectronic ions in solution, ca. 0.18 Å, is mainly due to the higher charge of thallium(III) and the contraction of the bonds due to the increased charge–dipole interaction. A similar contraction (ca. 0.16 Å) is found for the M–O distances in solution of the hexahydrated ions in the preceding row in the periodic table, Cd^{2+} and In^{3+}.[38]

We also attempted some EXAFS studies of mercury(II) pyridine and acetonitrile solvates. Spectra were recorded of saturated solutions of $Hg(CF_3COO)_2$ in pyridine and $Hg(CF_3SO_3)_2$ in pyridine and acetonitrile and of solid $[Hg(py)_2](CF_3SO_3)_2$. As a reference compound we used the hexasolvate, $[Hg(py)_6](CF_3SO_3)_2$, which has an unusual structure with the mercury atom in a distorted octahedral coordination of 6 N-atoms with two opposite Hg–N bonds slightly longer (average 2.50 Å at 183 K) than the other four (average 2.42 Å).[5]

As for the aqueous Hg^{2+} solutions, the amplitude of the EXAFS oscillations decreased very rapidly resulting in an almost featureless high k-region, thus giving very large Debye–Waller factors with correspondingly large uncertainties in the coordination numbers and distances. Similar observations have also been made in previous attempts to make structural studies of the solvation of mercury(II) in pyridine solution,[9] and the weak scattering effects in EXAFS and LAXS experiments are probably caused by disorder or fluxional coordination of the solvent molecules induced by SOJT vibronic couplings.

Thus, due to the intrinsic electronic character of the hexacoordinated mercury(II) ion in combination with limited concentrations, the EXAFS data did not allow determinations of the coordinated Hg–N distances in the acetonitrile- and pyridine-solvated Hg^{2+} ions. However, the XANES regions of the spectra

(20) (a) George, G. N.; Pickering, I. J. EXAFSPAK—A Suite of Computer Programs for Analysis of X-ray Absorption Spectra. SSRL; Stanford, CA, 1993. (b) Rehr, J. J.; Mustre deLeon, J.; Zabinsky, S. I.; Albers, R. C. *J. Am. Chem. Soc.* **1991**, *113*, 5135.
(21) Cramer, S. P.; Hodgson, K. O.; Stiefel, E. I.; Newton, W. E. *J. Am. Chem. Soc.* **1978**, *100*, 2748.
(22) Subramanian, V.; Seff, K. *Acta Crystallogr., Sect. B* **1980**, *36*, 2132.
(23) Braekken, H. *Z. Kristallogr.* **1932**, *81*, 152.
(24) Weber, G. *Acta Crystallogr., Sect. B* **1980**, *36*, 2779.
(25) Halfpenny, J.; Small, R. W. H.; Thorpe, F. G. *Acta Crystallogr., Sect. B* **1974**, *34*, 3075.
(26) Seccombe, R. C.; Kennard, C. H. L. *J. Organomet. Chem.* **1969**, *18*, 243.
(27) Chong, D. P.; Langhoff, S. R. *J. Chem. Phys.* **1986**, *84*, 5606.
(28) Pettersson, L. G. M.; Wahlgren, U.; Gropen, O. *Chem. Phys.* **1983**, *80*, 7.
(29) Faegri, K., Jr. Technical Note, Theoretical Chemistry. University of Oslo, Feb 1987, June 1987.
(30) Douglas, M.; Kroll, N. M. *Ann. Phys. (New York)* **1974**, *82*, 89.
(31) Hess, B. A. *Phys. Rev. A* **1989**, *33*, 3742.
(32) Almlöf, J.; Taylor, P. R. *J. Chem. Phys.* **1987**, *86*, 4070.
(33) Dunning, T. H., Jr. *J. Chem. Phys.* **1970**, *53*, 2823.
(34) Widmark, P. O.; Persson, B. J.; Roos, B. O. *Theoret. Chim. Acta* **1991**, *79*, 412.
(35) Huzinaga, S. Approximate Atomic Functions II. Department of Chemistry, University of Alberta, Edmonton, Alberta, Canada, 1971.
(36) Rafenetti, R. C. *J. Chem. Phys.* **1973**, *58*, 4452.
(37) Desclaux, J. P. *At. Data Nucl. Data Tabl.* **1973**, *12*, 311.
(38) Johansson, G. *Adv. Inorg. Chem.* **1992**, *39*, 159 and references therein.

can be used to obtain qualitative information on the coordination geometry around the mercury atom as discussed below (see part II. XANES).

$HgCl_2$. EXAFS data of aqueous mercury(II) chloride solutions were recorded both at Daresbury (SRS) and Stanford (SSRL). Satisfactory agreement was obtained by fitting model data for two Hg–Cl bonds at ca. 2.29(2) Å in both cases (the SRS data are displayed in Figure 1a).

For $HgCl_2$ in Me_2SO the Hg–Cl distance, 2.31(2) Å, is 0.02 Å longer than in water (the relative differences are more precise than the absolute accuracy in the bond lengths), reflecting the somewhat stronger solvation by the dimethyl sulfoxide molecules. This is consistent with the decrease of the Raman-active symmetric stretching vibrational frequencies, from 320 to 303 cm^{-1} in H_2O and Me_2SO, respectively.[10]

Compared to the model compound $HgCl_2(s)$ with Hg–Cl = 2.282 Å, the increase in the Hg–Cl bond distance is 0.01 Å (water) and 0.03 Å (Me_2SO), Table 1. The σ^2 values of the Hg–Cl bonds in the solvated $HgCl_2$ complexes were small, as for all HgX_2 complexes in this study, implying well-defined bonds as in the solid. Crystal structures of almost linear $HgCl_2$ molecules with weakly coordinated equatorial oxygen atoms (Hg–O = 2.7–2.9 Å) give a mean Hg–Cl distance of 2.305 Å,[39] and the increase by 0.02 Å from $HgCl_2(s)$ is consistent with the values obtained for the weakly solvated $HgCl_2$ molecules in solution. Attempts to include Hg–O distances in the refinements did not significantly improve the fits, however, and only for the Me_2SO solution approximate estimates of long Hg–O distances at ca. 2.6–2.7 Å with large σ^2 values could be obtained.

$HgBr_2$. The early crystal structure determination of the pure solid used as the model compound did not allow a precise determination of the Hg–Br distance, 2.49(10) Å.[24] By using the EXAFSPAK[20a] and FEFF[20b] programs with theoretical backscattering parameters a Hg–Br distance of 2.46(2) Å could be obtained for the solid $HgBr_2(s)$. The same procedure applied on the $TlBr_2^+$ complexes gave Tl–Br distances ca. 0.01 Å shorter than those obtained by the XFPAKG program system using model compounds.[14] The Hg–Br(aq) distance was evaluated to 2.42(2) Å, *i.e.* 0.04 Å shorter than in the solid but longer than in the gas phase, 2.383(8) Å.[40a] A crystal structure of an oligoether adduct with $HgBr_2$ displays 5 Hg–O distances ranging from 2.72 to 3.06 Å nearly perpendicular to an almost linear $HgBr_2$ group with the Hg–Br distances 2.387(3) and 2.409(3) Å.[41] This is in good agreement with the solution value for a weakly hydrated $HgBr_2$ molecule, considering that no bond length correction for thermal motion[42] was made in the crystal structure determination. Comparisons with other almost linear $HgBr_2$ molecules in solid solvates show rather large variations in the mean Hg–Br bond length, from 2.42 to 2.48 Å,[41] seemingly a result of equatorial interactions of different strengths with the mercury(II) atoms in the structures. This is probably also the reason for the shorter Hg–X distance in solution than in the solid for $HgBr_2$ but not for $HgCl_2$.

$Hg(CN)_2$(aq). A Hg–C distance of 2.04(2) Å with a coordination number of 2 was obtained, slightly longer than the value used for the solid model compound $Hg(CN)_2$ with Hg–C = 2.019 Å.[26] The Hg–N peak is enhanced by multiple scattering in the linear Hg–C–N group (Figure 1g), but a satisfactory fit is obtained with the backscattering parameters from the solid and the same distance 3.18(3) Å as in solution. No significant contribution from an Hg–O interaction could be detected in the EXAFS data.

TlX_2^+(aq). The Tl–X (X = Cl, Br, CN) distances are 0.07, 0.04, and 0.09 Å longer, respectively, in the TlX_2^+ complexes than for the corresponding isoelectronic HgX_2 species in solution (Table 1), which in view of the higher charge of thallium(III) seems surprising. However, mercury(II) is a very soft ion and the covalent contribution to the Hg–X bonds relative to the total bond energy is significantly larger as shown by the calculations (Table 3). As a consequence of the covalent bonding, the effective charge of the mercury atom becomes small (Table IIc), which leads to a weak hydration of the mercury(II) complexes. The

Table 2. Results of the Theoretical Calculations

(a) Optimized Geometries

system	distance	R_{SCF}/Å	R_{MCPF}/Å	R_{EXP}/Å
$Hg(CN)_2$	Hg–C	2.046	2.030	2.019[a]
	C–N	1.134	1.171	1.160[a]
$HgCl_2$	Hg–Cl	2.302	2.292	2.25–2.29[b]
$TlCl_2^+$	Tl–Cl	2.252	2.276	
$TlCl_2^+ \cdot 4H_2O$[c]	Tl–Cl	2.280		2.37
$Tl(CN)_2^+$	Tl–C	2.022	2.029	
$Tl(CN)_2^+ \cdot 4H_2O$[c]	Tl–C	2.046		2.11
HCN	C–H	1.052	1.069	1.063[d]
	C–N	1.124	1.163	1.153[d]
HCl	H–Cl	1.270	1.281	1.274[e]

(b) Excitation Energies[f]

system	transition	ΔE(MCPF)/eV
$Hg(CN)_2$	$(2p) \rightarrow \Sigma^+_g$	5.91
	$(2p) \rightarrow \Pi_g$	2.51
$HgCl_2$	$(2p) \rightarrow \Sigma^+_g$	7.29
	$(2p) \rightarrow \Pi_g$	0.16

(c) Mulliken Populations[g]

system		M	C	N	Cl	H
$Hg(CN)_2$	s	3.27	3.25	3.70		
	p	6.43	2.79	3.37		
	d	9.74	0.07	0.05		
	f	0.11				
	q	+0.45	–0.11	–0.12		
$HgCl_2$	s	3.06			5.93	
	p	6.46			11.23	
	d	9.80			0.12	
	f	0.12				
	q	+0.56			–0.28	
$TlCl_2^+$	s	3.29			5.93	
	p	6.74			10.92	
	d	9.89			0.12	
	f	0.13				
	q	+0.95			+0.03	
$Tl(CN)_2^+$	s	3.37	3.20	3.75		
	p	6.75	2.77	3.12		
	d	9.85	0.06	0.06		
	f	0.12				
	q	+0.91	–0.03	0.07		
HCN	s		3.21	3.71		0.82
	p		2.78	3.34		0.02
	d		0.07	0.05		
	q		–0.06	–0.11		0.16
HCl	s				5.92	0.68
	p				11.18	0.10
	d				0.13	
	q				–0.23	0.23

[a] Corrected for thermal motion.[26] [b] Reference 44, gas-phase values. [c] Equatorial water molecules represented by point charges (O, –0.4; H, +0.8) at expected atomic positions, d(Tl–O) = 2.41 Å ($Tl(CN)_2^+$) and 2.32 Å ($TlCl_2^+$), experimental value; see Table 1. [d] Reference 45. [e] Reference 40b. [f] Calculated difference from the 2p ionization energy. [g] Total s, p, d, and f populations of the natural orbitals and gross atomic charges *q* obtained from the MCPF calculations at optimized geometries.

(39) Iwamoto, R. *Bull. Chem. Soc. Jpn.* **1973**, *46*, 1114, 1123.
(40) Landolt-Börnstein, *Numerical Data and Functional Relationships in Science and Technology, New Series, Group II: Atomic and Molecular Physics*; Hellwege, K.-H., Hellwege, A. M., Eds.; Springer: Berlin, 1987: (a) Vol. 21, p 43; (b) Vol. 15, p 163.
(41) (a) Frey, M. *C. R. Acad. Sci. Ser. C* **1970**, *270*, 1265. (b) Frey, M.; Monier, J. C. *Acta Crystallogr., Sect. B* **1971**, *22*, 2487. (c) Leligny, H.; Frey, M.; Monier, J. C. *Acta Crystallogr., Sect B* **1972**, *28*, 2104. (d) Brodersen, K.; Frohring, H. M.; Thiele, G. *Z. Anorg. Allg. Chem.* **1981**, *483*, 86.
(42) Trueblood, K. N. In *Accurate Molecular Structures*; IUCr Monographs on Crystallography, No. 1; Domenicano, A., Hargittai, I., Eds.; Oxford University Press: Oxford, U.K., 1992; Chapter 8.

Table 3. CSOV Analyses of $Hg(CN)_2$ and $Tl(CN)_2^+$

step	ΔE/kJ mol^{-1}	ΔE/%
	$Hg(CN)_2$[a]	
1. Coulombic energy	1637.02	68.7
2. ion polarizability	325.18	13.6
3. "π-bonding"	16.11	0.7
4. σ-bonding	382.44	16.0
5. d $\rightarrow$ π^* back-bonding	23.39	1.0
total binding energy	2384.1	100
	$Tl(CN)_2^+$[b]	
1. Coulombic energy	2734.26	67.0
2. ion polarizability	751.37	18.4
3. "π-bonding"	43.43	1.1
4. σ-bonding	529.10	13.0
5. d $\rightarrow$ π^* back-bonding	21.50	0.5
total binding energy	4079.7	100

[a] R(Hg–C) = 2.046, R(C–N) = 1.171 Å. [b] R(Tl–C) = 2.022, R(C–N) = 1.171 Å.

higher effective charge on the thallium atom of the TlX_2^+ species (Table IIc) leads to a stronger hydration in solution. This is reflected by the fairly well-defined Tl–O distances obtained from EXAFS data for assumed pseudo-octahedral $[TlX_2(H_2O)_4]^+$ complexes (Tl–O ~ 2.32, 2.38, and 2.42 Å for X = Cl, Br, and CN, respectively)[14] and corresponds to the lengthening observed of the Tl–X bonds in solution (cf. Tables 1 and 2a). Possible differences in coordination geometry in solution should also be considered. For HgX_2 small deviations from a linear toward a pseudotetrahedral structure are possible as judged from the changes in the vibration stretching frequencies, which may be used to estimate an X–Hg–X angle of ~160° for both $HgCl_2$ and $HgBr_2$ in aqueous solution.[10]

II. XANES. The structure of the absorption edge, in this case Hg L_{III} (12.28 keV for the metal),[43] offers qualitative information about the coordination geometry around the absorbing atom,.[18b-d] Figure 2A shows XANES spectra of the samples studied, including the pyridine and acetonitrile solutions. Some thallium(III) samples have also been included, with a shift of the energy scale by 372 eV for TlX_2^+ and 366 eV for $Tl(CN)_2^+$(aq); the Tl L_{III} edge is at 12.66 keV for the metal.[43] The negative second derivatives are also shown in Figure 2B in order to visualize weak features in the absorption edges.

The XANES region can be divided into a "discrete part" below and a "continuum part" above the threshold E_0 ionization energy.[18c] The energies of the bound excited states in the discrete part are our main concern here. In particular, interatomic transitions to Rydberg-like states are expected to be found in the "threshold" or low-energy part of the XANES region, while transitions to valence orbitals and bound resonances due to multiple scattering processes are dominant at higher energies. This is also what makes XANES informative about the coordination geometry.[18c] The close similarity between the solution and solid-state spectra (Figure 2) shows, however, that the multiple scattering resonances in this case are given mainly by the well-defined intramolecular structure in the complexes, with small contributions from the surrounding atoms.

A pre-edge transition occurs at ca. 12 282–3 eV (12 286 for the cyanides) for all the mercury(II) samples (Figure 2). The high intensity and the similar energy of this transition indicate that it is electric-dipole allowed and corresponds to a bound final state. Possible assignments therefore include 2p $\rightarrow$ 6s (Hg) and 2p $\rightarrow$ ligand orbitals.

In general, the intensity of the ~12 283-eV transition decreases with increasing coordination around the metal ion, *i.e.* linear > tetrahedral > octahedral, probably due to a more Rydberg-like character of the excited orbitals for the higher coordination

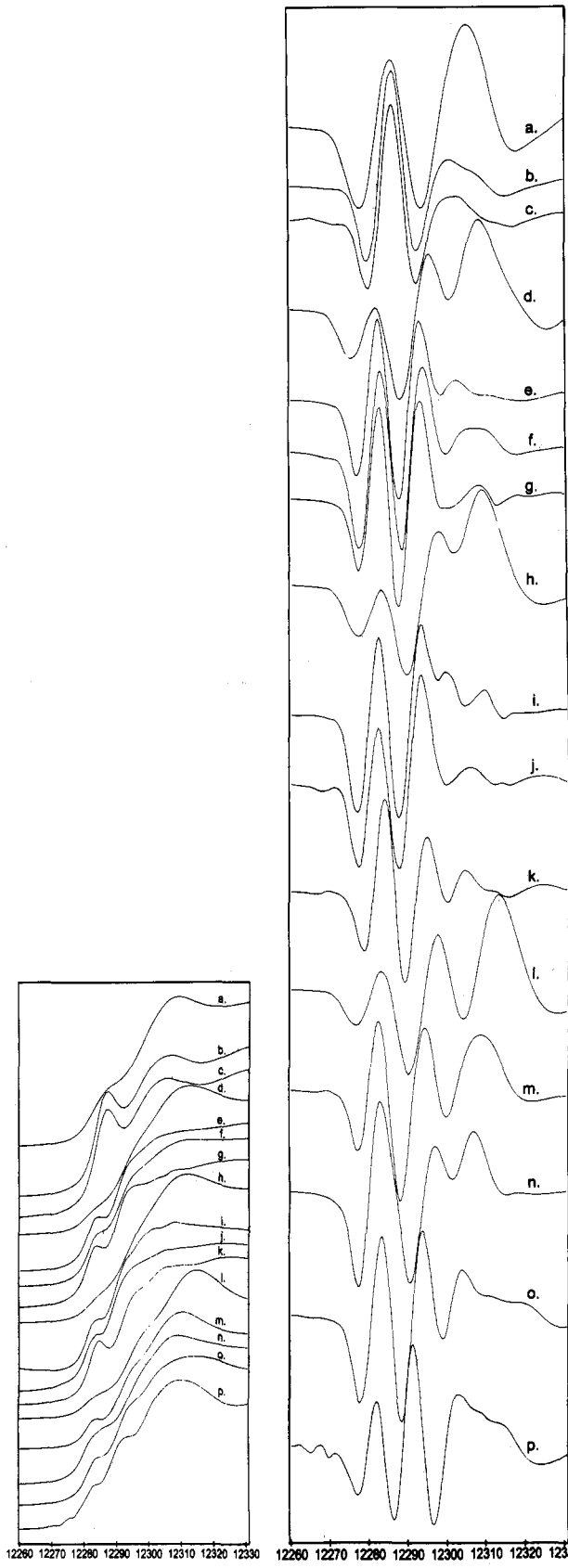

Figure 2. XANES of (A, left) absorption edges and (B, right) negative second derivatives: (a) $Tl(CN)_2^+$(aq); (b) $Hg(CN)_2$(aq); (c) $Hg(CN)_2$(s); (d) $TlCl_2^+$(aq); (e) $HgCl_2$(aq); (f) $HgCl_2(Me_2SO)$; (g) $HgCl_2$(s); (h) $TlBr_2^+$(aq); (i) $HgBr_2$(aq); (j) $HgBr_2$(s); (k) $Hg(py)_2(CF_3SO_3)_2$; (l) Tl^{3+}(aq); (m) Hg^{2+}(aq); (n) $Hg^{2+}(CH_3CN)$; (o) Hg^{2+}(py); (p) $Hg(py)_6(CF_3SO_3)_2$. The energy scale is offset by 372 eV for $TlCl_2^+$(aq) and $TlBr_2^+$(aq) and by 366 eV for the $Tl(CN)_2^+$(aq) solution.

numbers. Similar observations have also been made for a number of halide complexes of copper(I), another d^{10} ion,[16] although the

(43) *Practical Handbook of Spectroscopy*; Robinson, J. W., Ed.; CRC Press: Boca Raton, FL, 1991.

selection rules are different for a Cu Kα excitation. The weakest intensity is thus found for the 6-coordinate solvates, $Hg^{2+}(aq)$, $Hg^{2+}(CH_3CN)$, $Hg^{2+}(py)$, and $Tl^{3+}(aq)$ (Figure 2l-o). The spectra of the MX_2 (M = Tl, Hg; X = Cl, Br) species (Figures 2d-j) are very similar after the 372-eV shift of the Tl scale. Somewhat enhanced intensities of the ~12 283-eV transitions can be seen for the spectra of $HgCl_2$ and $Hg(py)_2^{2+}$ complexes in the solid state as compared to the solvated complexes (Figure 2g,k). This is possibly connected with more well-defined and stronger equatorial interactions around the mercury atom in the solids.

The edge structure of the cyanide complexes shows considerable differences. The $Hg(CN)_2(aq)$ and $Hg(CN)_2(s)$ complexes with nearly identical XANES spectra (Figure 2a,b), and likewise the corresponding $Tl(CN)_2^+$ complexes, display a much higher intensity of the broad first pre-edge peak than the other HgX_2 complexes with the band maximum shifted to ca. 12 286 eV. It has been shown that the CN ligands in the octahedral $Fe(CN)_6^{n-}$ ($n = 3, 4$) complexes give two strong and relatively sharp features in the XANES spectra separated by ca. 17 eV, which are associated with the multiple scattering shape resonances within the CN ligands.[18d] A comparison with the $Tl(CN)_2^+(aq)$ spectrum (Figure 2a, scale offset 366 eV) reveals a similar pattern, although the first peak now is clearly split into two components and the separation between the major bands is ca. 20 eV as compared to ca. 17 eV for $Hg(CN)_2$. In calculated $Fe(CN)_6^{4-}$ spectra a similar splitting of the first peak resulted from a distortion of the coordination shell, but the separation of the two major bands was found to depend mainly on the C–N distance.[18c,d] These results are consistent with the differences found in the solution structures of the weakly hydrated $Hg(CN)_2$ with a strong C–N bond (cf. Vibrational Force Constants) and the more strongly hydrated $Tl(CN)_2^+$ complex with probably a pseudo-octahedral Tl coordination.[14] However, a contribution to this splitting of the first pre-peak may also be due to the close (2p) $\rightarrow \Sigma_g^+$ and (2p) $\rightarrow \Pi_g$ transitions calculated for the $Hg(CN)_2$ complex (see Transition Energies).

A second pre-edge transition, which seems to be connected with the strongly coordinating pyridine ligand, occurs at ca. 12 293 eV for $Hg^{2+}(py)$, $[Hg(py)_2](CF_3SO_3)_2$, and $[Hg(py)_6](CF_3SO_3)_2$ (Figure 2k,o,p), and a possible assignment is Hg 2p $\rightarrow \pi^*(py)$ for a bound-state transition (see Transition Energies). A similar feature is also evident for $HgCl_2(s)$ but at a slightly lower energy, 12 293 eV (Figure 2e), but is more likely in this case to be a multiple scattering resonance because of the more rigid and closer equatorial Hg···Cl interactions.

The solvated Hg^{2+} ion has a different edge structure in acetonitrile with only one prominent pre-edge transition at ca. 12 283 eV (Figure 2n) than in water and pyridine where a second transition occurs at 12 292–3 eV (Figure 2m,o). In acetonitrile the peak is broader with a somewhat higher intensity than for the other solvents, which probably is connected with enhanced multiple-scattering effects by the linear Hg–N–C entities.

III. Theoretical Calculations. The aim of the theoretical calculations was to obtain additional information about the differences in bonding between the isoelectronic mercury(II) and thallium(III) complexes with cyanide or halide (represented by Cl^-) ligands. In particular an explanation was sought for the differences between the XANES spectra of $HgCl_2$ (or $HgBr_2$) and $Hg(CN)_2$, cf. Figure 2. In Table 2 the results of the theoretical calculations on $Hg(CN)_2$, $HgCl_2$, $Tl(CN)_2^+$, $TlCl_2^+$, HCN, and HCl species are summarized. The optimized SCF and MCPF geometries are given in Table 2a, the calculated electronic transitions in Table 2b, and Mulliken population analyses in Table 2c.

Electronic and Geometrical Structures. An accurate description of dynamical correlation effects is essential for the bond distances in the mercury(II) and thallium(III) complexes. This was evident in the first attempt to construct an ECP potential for the mercury atom when the Hg basis set was constructed from the SCF orbitals, which resulted in MCPF level Hg–C and Hg–Cl distances approximately 0.1 Å longer than those obtained experimentally. A mercury valence basis using atomic natural orbitals (ANO) with explicit inclusion of the 5f orbital significantly reduced the Hg–C and Hg–Cl distances to values only slightly (0.01–0.04 Å) longer than the experimental ones. The ANO basis sets were considered suitable for relative comparisons of transition energies.

The optimized geometry for $Hg(CN)_2$ gives Hg–C = 2.030 Å and C–N = 1.171 Å at the MCPF level. In order to compare the C–N bond with a system without the possibility of π back-donation from metal d orbitals, similar calculations were performed on HCN, giving an optimized C–N distance of 1.163 Å. The slightly longer C–N bond in $Hg(CN)_2$ is related to the participation of the π^*(C–N) orbital in the bonding. The admixture of ligand π^* character in the orbitals is also reflected by the slight decrease obtained for the overlap populations for the C–N bonds in HCN (+1.68) and $Hg(CN)_2$ (+1.62). In the excited 2p $\rightarrow \pi^*$ state of $Hg(CN)_2$ the corresponding overlap is reduced to only +0.41.

For $HgCl_2$ the computed Hg–Cl distance, 2.292 Å, is longer than the most precisely determined experimental gas-phase value (2.252 ± 0.005 Å)[44] but close to that of the $HgCl_2(aq)$ complex (2.29 Å). Correlation effects were found to have an appreciable influence on the calculated distances, in particular for $Hg(CN)_2$. The Hg–C distance was reduced by 0.016 Å in comparison with the SCF results (Table 2a). The C–N bond, which becomes slightly weakened by the influence of the antibonding orbital, was elongated by a similar amount. The bond lengths in HCl and HCN are within 0.01 Å from the experimental gas-phase values.[40b,45]

The molecular orbital energy level diagrams for neutral $Hg(CN)_2$ and $HgCl_2$, as derived from the SCF level calculations, are shown in Figure 3. The symmetry of the HOMO is σ_g (mainly Cl $3p_{x,y}$) for $HgCl_2$ and π_g (C–N p_π) for $Hg(CN)_2$. However, the symmetry of the LUMO is different in the two cases: π_u (~C $3p_{x,y}$) and σ_g (~Hg 6s), for $Hg(CN)_2$ and $HgCl_2$, respectively, and the Hg 2p $\rightarrow$ LUMO transition is thus only dipole allowed in the latter case. For $Hg(CN)_2$ the first dipole-allowed transition occurs to the second virtual orbital which is of σ_g symmetry.

The differences between the $Hg(CN)_2$ and $HgCl_2$ systems are partly due to the different electronegativities of the ligand atoms, as seen by the gross atomic charges; see Table 2c. The Mulliken population analyses show the Hg–Cl bond to be more polar than the Hg–C bond. For $Hg(CN)_2$ the charge on the mercury atom was slightly lower, +0.45, than in $HgCl_2$, +0.56. The low charges are consistent with the covalent character of the Hg–X bonds, in particular for the cyanide complex. Actually, the charges obtained for the mercury atom are rather similar to those obtained for hydrogen in the reference compounds: +0.17 (HCN) and +0.23 (HCl).

In the ground state of $Hg(CN)_2$ there is some contribution of π-back-bonding, *i.e.* donation from metal dπ to empty ligand π^* orbitals. The contribution is as expected rather small (the π^* coefficients of the natural orbitals are only ~0.07) because of (1) the divalent oxidation state of the metal ion and (2) the negatively charged CN^- ligands. Both these conditions are unfavorable for a high amount of π-back-bonding in the system, as discussed in textbooks.[46]

(44) (a) Kashiwabara, K.; Konaka, S.; Kimura, M. *Bull. Chem. Soc. Jpn.* **1973**, *46*, 410. (b) Gershikov, A. G.; Spiridonov, V. P. *J. Mol. Struct.* **1981**, *75*, 291.
(45) (a) Simmons, J. W.; Anderson, W. E.; Gordy, W. *Phys. Rev. 77*, 77; Erratum **1952**, *86*, 1055. (b) Nethercot, A. H., Jr.; Klein, J. A.; Townes, C. H. *Phys. Rev.* **1952**, *86*, 798L.
(46) Huheey, J. E.; Keiter, E. A.; Keiter, R. L. *Inorganic Chemistry*, 4th ed.; Harper Collins: New York, 1993; Chapter 11.

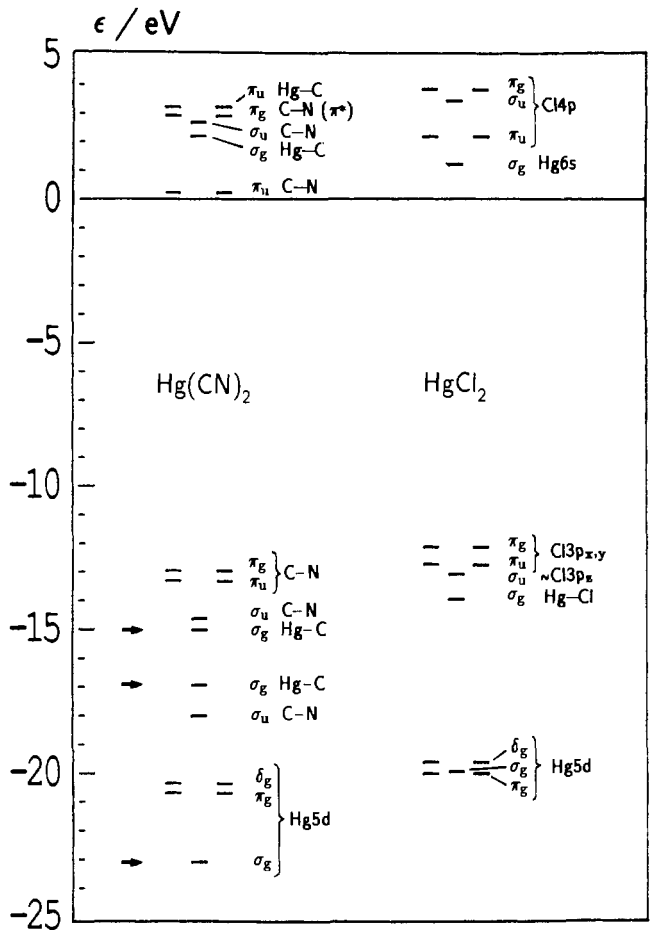

Figure 3. MO energy level diagram derived from the *ab initio* SCF calculations on neutral $Hg(CN)_2$ (left) and $HgCl_2$ (right) molecules. The electronic transitions from the Hg 2p level to the σ_g and π_g orbitals are dipole allowed. The arrows to the left mark the three σ_g orbitals plotted in Figure 4.

A comparison between the calculated parameters for the isoelectronic MX_2 (X = Cl^-, CN^-) complexes of the Hg^{2+} and Tl^{3+} ions displays some notable features. Due to the higher charge shorter M–Cl and M–CN distances are expected in the thallium(III) complexes. However, the difference is reduced to 0.016 Å for the chloride complexes and for the cyanide complexes the M–C distances are virtually equal. The $5d_{z^2}$-6s mixing is more efficient for mercury(II) than for thallium(III), because of the higher stability of the 5d orbital in thallium. The separations between the atomic 5d and 6s orbitals, as measured by the differences in orbital energies for the isolated ions, are 18.53 eV for Hg^{2+} and 23.87 eV for Tl^{3+}. The three bonding σ_g orbitals are illustrated for $Hg(CN)_2$ in the electron density plot in Figure 4. The corresponding plot for the σ_g orbitals of $Tl(CN)_2^+$ (not shown) looks qualitatively similar but has a higher maximum electron density localized at the metal atom, 1.13 and 0.85 e/(bohr)^3 for thallium and mercury, respectively. A higher degree of covalency and charge transfer in the bonding of the mercury(II) complexes is thus the probable reason for the small differences in bond length despite the higher charge of thallium(III).

The calculated bond distances for the thallium(III) complexes are, however, shorter than the experimental EXAFS results in solution, cf. Tables 1 and 2a. This can be explained by the relatively strong hydration. As a first crude attempt to estimate the effects of the water molecules in the first coordination shell, we made SCF calculations on pseudo-octahedral $TlX_2^+ \cdot 4H_2O$ complexes, with the equatorial water molecules represented by point charges (O, –0.8, and H, +0.4, corresponding to a dipole moment of ~2.5 D) at the expected atomic positions. Despite

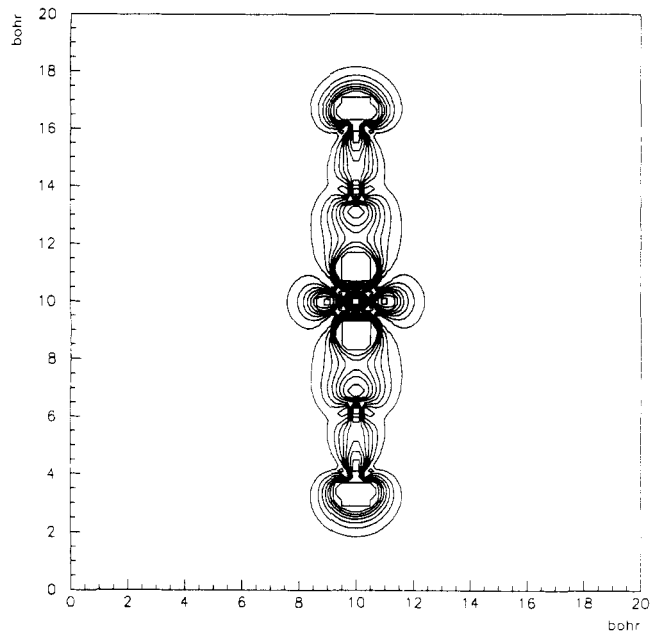

Figure 4. Electron density plot (maximum contour 0.85 e/(bohr)^3, step 0.014; 1 bohr = 0.529 177 Å) of the three bonding σ_g molecular orbitals marked in Figure 3 for the N–C–Hg–C–N molecule (σ_g; Hg 5d and $2\sigma_g$; Hg–C) showing the effect of $5d_{z^2}$–6s mixing on the Hg atom.

the simple model significant increases of the Tl–C and Tl–Cl bond distances were obtained (Table 2a).

CSOV Analyses. In order to make a more detailed study of the differences in bond character between the $Hg(CN)_2$ and $Tl(CN)_2^+$ complexes, and in particular to investigate the contribution from 5d → $\pi^*(CN^-)$ back-donation, a constrained space orbital variation (CSOV) analysis was applied;[47] see Table 3. This method basically consists of a sequence of SCF calculations, where the orbitals of the fragments (*i.e.* Hg^{2+} and CN^-) are generated at an infinite distance and then brought to the bonding distance (for optimized SCF geometry), at which the orbital relaxation is extended stepwise with evaluation of the successive energy gains. The sums of all terms should equal the total complex binding energy, *i.e.* $\Delta E = E\{Hg^{2+}\} + 2E\{CN^-\} - E\{Hg(CN)_2\}$, which is 2384 and 4080 kJ mol^{-1} for $Hg(CN)_2$ and $Tl(CN)_2^+$, respectively. The first step in the analysis (see Table 3) describes the electrostatic (Coulomb) attraction, and the second step, the contribution from the ligand polarizability. In these two steps the occupied metal orbital functions are kept frozen and the virtual metal functions deleted. As expected from the higher charge, these terms are approximately twice as large for the thallium complex and contribute by 85.4% (82.3% for $Hg(CN)_2$) to the total binding energy (assuming a dissociation into ionic products). The third step involves the complete mixing of the Hg $p_{x,y}$, d(δ), and f orbitals with the corresponding ligand orbitals, which only gives slight energy gains indicating minor π (and δ) bonding contributions. The fourth step involves the mixing of orbitals responsible for a σ overlap, σ_g and σ_u, which is the overwhelming part of the covalent contribution. Finally, the π back-donation orbitals, π_g, are included, which shows a slightly larger absolute energy gain for $Hg(CN)_2$ (23.4 kJ mol^{-1}) than for $Tl(CN)_2^+$ (21.5 kJ mol^{-1}). One can also compare the back-bonding contribution with the total covalent bonding (the sum of steps 3–5). The relative contribution is higher for $Hg(CN)_2$ (5.5%) than for $Tl(CN)_2^+$ (3.6%) and indicates that the back-donation, although still relatively small, is more important in the Hg–CN bonding.

Vibrational Force Constants. The significance of the above results is clearly seen in comparisons of the M–C and C–N

(47) Bagus, P. S.; Hermann, K.; Bauschlicher, C. W. *J. Chem. Phys.* **1984**, *80*, 4378.

stretching force constants, f_r and f_R, respectively, from force field analyses of vibrational spectra of the isoelectronic $[Au(CN)_2]^-$, $[Hg(CN)_2]$, and $[Tl(CN)_2]^+$ complexes.[14] The values obtained are for f_r = 2.73, 2.52, and 2.38 N cm^{-1} and for f_R = 17.72, 18.20, and 17.76 N cm^{-1}, respectively. The decreasing f_r values from gold to thallium reflect a sharper curvature around the minimum of the bonding energy curve to the left in the sequence (despite the decrease in the total bonding energy). This is caused by the relatively larger covalent contribution to the bond displacing the minimum and contracting the interatomic distance as shown by the experimental M–C bond lengths, 2.11 Å in $Tl(CN)_2^+$(aq),[14] 2.02 in $Hg(CN)_2$(s),[26] and 1.97 Å in Tl[$Au(CN)_2$](s) and Cs-[$Au(CN)_2$](s).[48] This is contrary to what is expected if only the decreasing charge of the isoelectronic metal atoms is considered, although in condensed phases a higher metal charge will be somewhat reduced by increasing solvation or other equatorial interactions with surrounding atoms. However, the calculations show a similar effect for the isolated $Hg(CN)_2$ and $Tl(CN)_2^+$ species with much higher total binding energy for thallium, although the calculated Tl–C bond distance (2.022 Å) now is slightly shorter than the Hg–C distance (2.046 Å), Table 3. The comparison of the experimental values shows that the relative importance of the covalency in the bonding must be even higher for gold(I) than for mercury(II).

The highest f_R value, corresponding to the strongest C–N bonding, is found for $[Hg(CN)_2]$. This probably arises from a balance between two effects, as discussed in Ref 49. A stronger M–C σ bond results in a more symmetrical and stronger C–N bonding, and the charge transfer reduces the charge difference between the M^{n+} ion and the CN^- ligands (cf. Table 2). This, however, facilitates back-bonding from the metal atom d to antibonding ligand π orbitals (cf. Table 3), which weakens the C–N bonds. High covalency (particularly in $[Au(CN)_2]^-$) giving strong σ bonding would then result in a high degree of back-bonding. The maximal C–N bond strength then occurs in $[Hg(CN)_2]$, which has lower covalency in the M–C bond but also a smaller amount of back-bonding than $[Au(CN)_2]^-$. Further investigations of the bonding in these systems are in progress.

Transition Energies. The energies of the two lowest-lying electronic transitions from the 2p(Hg) level relative to the (2p) ionization energy (used to define the position of the L_{III} absorption edge) have been calculated for $Hg(CN)_2$ and $HgCl_2$ by MCPF methods (Table 2b). According to the calculations, the ionization limit should correspond to approximately 12 290 eV. The transitions to higher-lying orbitals in Figure 3 (ϵ > 4 eV) are above the ionization limit and would correspond to unbound states.

A qualitative correspondance between the first allowed transitions and the positions of the pre-edge XANES peaks (Figure 2a-g) is found. The main pre-edge peak at ~12 283 eV corresponds to the calculated energy for a (2p) → Σ_g^+ transition for the $HgCl_2$ complexes, and the weak feature at ~12 293 eV for the solvated $HgCl_2$ complexes in H_2O and Me_2SO (Figure 2e,f) is possibly related to a (2p) → Π_g transition, although the energy differences are not perfectly reproduced. The broad, slightly asymmetric prepeak for $Hg(CN)_2$ at ~12 286 eV seems consistent with the two compoonents arising from the (2p) → Σ_g^+ and (2p) → Π_g transitions, 2.5 and 5.9 eV below the ionization limit, respectively. However, these transition features are probably overlapped by the strong multiple scattering resonance between the C–N atoms, as discussed in part II. XANES above.

Acknowledgment. The continuing support of the Swedish Natural Science Research Council is gratefully acknowledged. Dr. Britt Hedman's expertise and excellent organization of the SSRL XAFS experimental stations have been highly appreciated. We wish to thank Prof. R. A. Scott, University of Georgia, for our use of the XFPAKG programs, Drs. G. N. George and I. J. Pickering for our use of the EXAFSPAK program system, Dr. Per Persson for his kind help with the XAFS calculations and for helpful discussions on sources of error in interpretations of XAFS spectra, and Prof. János Mink, University of Veszprém, for providing us with results from the force field calculations.

(48) Blom, N.; Ludi, A.; Bürgi, H.-B.; Tichy, K. *Acta Crystallogr., Sect. C* **1984**, *40*, 1767.
(49) Jones, L. H. *Inorganic Vibrational Spectroscopy*; Marcel Dekker: New York, 1971; Chapter 4.